

# Lasing in an Assembled Array of Silver Nanocubes

*Mindaugas Juodėnas<sup>1</sup>, Nadzeya Khinevich<sup>1</sup>, Gvidas Klyvis<sup>1</sup>,  
Joel Henzie<sup>2</sup>, Tomas Tamulevičius<sup>1</sup>, Sigitas Tamulevičius<sup>1</sup>*

## Abstract

We demonstrate a surface lattice resonance (SLR)-based plasmonic nanolaser that leverages bulk production of colloidal nanoparticles and assembly on templates with single particle resolution. SLRs emerge from the hybridization of the plasmonic and photonic modes when nanoparticles are arranged into periodic arrays and it can provide feedback for stimulated emission. It has been shown that perfect arrays are not a strict prerequisite for producing lasing. Here, we propose using high-quality colloids instead. Silver colloidal nanocubes feature excellent plasmonic properties due to their single-crystal nature and low facet roughness. We use capillarity-assisted nanoparticle assembly to produce substrates featuring SLR and comprising single nanocubes. Combined with a laser dye pyromethene-597, the nanocube array lases at 574 nm with <1.2 nm linewidth, <100  $\mu\text{J}/\text{cm}^2$  lasing threshold, and produces a beam with <1 mrad divergence, despite less-than-perfect arrangement. Such plasmonic nanolasers can be produced on a large-scale and integrated in point-of-care diagnostics, photonic integrated circuits, and optical communications applications.

## Introduction

The demand for miniaturization and improved efficiency of coherent light-emitting devices has steadily increased over time.<sup>1</sup> Small lasers operating at the nanoscale can benefit applications such as optical communications, sensing, bioimaging, photonic circuits, etc.,<sup>2</sup> where a superior size-to-efficiency ratio and decrease in power requirements is particularly attractive. Making nanolasers requires ultimate control of light fields at the nanoscale, and metasurfaces, 2D collections of nanostructures, are excellent at this task. In particular, plasmonic metasurfaces enable precise control over light-matter interactions leading to enhancements in light emission, confinement, and manipulation by squeezing electromagnetic fields to subwavelength scales in the near field.<sup>3</sup>

Plasmonic metasurfaces can feature surface lattice resonances (SLRs) - collective in-phase excitations formed by localized surface plasmons (LSP) of nanoparticles and diffractive photonic modes of the lattice. These SLRs have been extensively studied and reviewed.<sup>4</sup> One of the applications of these hybrid plasmonic-photonic modes is light amplification and stimulated emission.<sup>1,5,6</sup> When a SLR-supporting plasmonic system is in contact with a medium that can provide gain, the lattice resonance acts as a feedback mechanism, amplifies photoluminescence (PL) and

can generate light that is both spatially and temporally coherent.

The first SLR-based nanolasers were made using electron beam deposited gold<sup>7</sup> and silver<sup>8</sup> nanocylinders and organic dyes. Subsequent research expanded on this foundation to achieve wavelength tunability via refractive index<sup>9</sup> and stretching of elastomer substrates,<sup>10</sup> direction of emission control via multiple lattice modes,<sup>11-13</sup> and switching using magnetic fields.<sup>14</sup> Apart from dyes, quantum dots<sup>15-18</sup> and up-converting nanoparticles<sup>19</sup> have also been used as gain materials. Emission wavelengths from UV using aluminum nanoparticles to NIR using gold have been demonstrated, and a combination thereof accomplished white-light lasing.<sup>20</sup>

While most reported SLR-based nanolasers are fabricated using either e-beam lithography<sup>7,9,12,14,20-22</sup> or the PEEL method (a combination of phase-shifting photolithography, etching, electron-beam deposition and lift-off of the film),<sup>23</sup> recent studies have shown that nanolasing can still occur even when a significant fraction of nanoparticles is absent from the array or the lattice order is decreased.<sup>12,24,25</sup> Interestingly, removing some fraction of particles can even help to outcouple light and increase the slope of the input-output curve while maintaining a similar threshold.<sup>25</sup> This intriguing finding suggests that defect-free lattice

fabrication through lithography may not be strictly necessary and opens the door to bottom-up methods that can offer improved scalability and cost at the expense of accuracy and precision.

An attractive prospect in this regard is the use of colloidal nanoparticles.<sup>26</sup> Highly crystalline colloids can be synthesized at a large scale.<sup>27</sup> Crystallinity ensures superior scattering-to-absorbance ratios versus physically deposited polycrystalline materials with grain boundaries and rough facets that generate absorptive damping.<sup>28,29</sup> Furthermore, these colloids are available in a variety of shapes, which could enable intelligent engineering of hot spots and facilitate anisotropic Purcell enhancement of the gain media for tunable devices.<sup>30,31</sup> The challenge then lies in arranging these nanoparticles in a manner conducive to providing lasing feedback.

Template-assisted nanoparticle assembly is a robust technique that can address this task. A variation of it has been used to produce a colloid-based nanolaser, where drop casting in combination with stamping of a patterned elastomer mold yielded clusters of nanoparticles.<sup>32</sup> Capillarity-assisted particle assembly (CAPA) is another variation that allows a high degree of control of the number of particles per unit cell, down to single particle precision.<sup>32,33</sup> In earlier work, we have shown that this method can produce nanoparticle assemblies on a large scale ( $>1\text{ cm}^2$ ) and can feature high-quality SLRs.<sup>26,34</sup>

In this study, we exploit the template-assisted approach to fabricate nanolasers using single, monocrystalline Ag nanocubes arranged in a subwavelength lattice (**Figure 1**). By leveraging CAPA we successfully formed square plasmonic arrays featuring a sharp SLR. We then demonstrate lasing in the presence of a fluorescent dye with a threshold comparable to that of substrates developed using lithography-based methods. We comprehensively characterize the lasing emission, including parameters such as emission spectra, threshold, beam profile, and polarization.

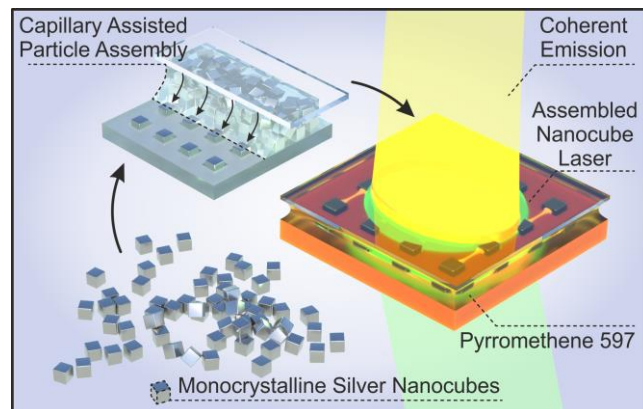


**Figure 1. Nanolaser based on assembled colloidal nanoparticles.** Schematic of an optically pumped nanolaser device comprising a self-assembled array of monocrystalline Ag nanocubes and organic dye. When pumped beyond the threshold using 515 nm light, the device lases at 574 nm, consistent with the fluorescence of the pyrromethene-597 dye and surface lattice resonance-based feedback.

## Results

### SLR-based feedback design and nanolaser fabrication

*Nanolaser design.* The design of a nanolaser with SLR-based feedback, not unlike any other optically pumped laser, requires a good match between material properties and excitation conditions. Achieving population inversion and stimulated emission at the designed wavelength relies on engineering a spectral overlap of the three major components: the pump needs to coincide sufficiently with the absorption of the gain medium, and the photoluminescence (PL) of the gain needs to match the resonant frequency of the resonator. We chose the pumping source to be our entry point to this problem and opted to use the second harmonic of Yb:KGW laser at 515 nm, emitting 270 fs pulses. Pyrromethene 597<sup>35,36</sup> (P597) was then an excellent spectral match for the pump wavelength with a high conversion rate ( $>30\%$ ) and a proven track record as a laser dye.<sup>37,38</sup> P597 has a strong emission peak centered at  $\sim 580\text{ nm}$ , which is attainable for silver photonics.

The next step is designing the feedback mechanism, which in this case is the SLR of the plasmonic Ag nanocube array. The empty lattice band structure (**Figure 2A**) of a square array with a periodicity of 400 nm in the PDMS environment ( $n = 1.42$ ) features a flat band (zero group velocity) at the  $\Gamma$  point with a wavelength of  $\sim 562\text{ nm}$ , matching the PL of the dye (**Figure 2B**). A high density of optical states is thus expected at this point, which may be sufficient to provide lasing feedback.<sup>7</sup> We then

populate this lattice using plasmonic nanoparticles to form a high-quality SLR.

The quality factor of the SLR is highest when the localized surface plasmon resonance (LSPR) of individual nanoparticles is somewhat blue-shifted with respect to the Rayleigh anomaly (RA) of the lattice (marked as solid lines in **Figure 2A** and dashed lines in **Figures 2C, D**). Since we have established the spectral location of the flat band in the previous step, the target is to find nanoparticles with a blue-shifted scattering peak and minimal absorption. We use Ag nanocubes because they can be synthesized in a monocrystalline form with smooth facets and we expect them to have an improved scattering-to-absorbance ratio compared to vacuum-deposited material.<sup>39</sup> We ran electromagnetic calculations

using a nanocube geometry and found that  $a = 65$  nm edge length particles will fit the scattering requirement (blue shift with respect to the RA) very well (**Figure 2C** shows the calculated scattering cross-section). In subsequent calculations, we set periodic boundary conditions with a periodicity of 400 nm. Unsurprisingly, the system features a strong resonance at 581 nm (**Figure 2D**), and the electric field intensity distribution at this wavelength (**Figure 2E**) showed a standing wave pattern as well as strong hot spots around the nanoparticles, characteristic of the delocalized photonic-plasmonic SLR mode. The calculated dip in transmittance has a FWHM of  $\sim 5.8$  nm, resulting in a theoretical  $Q$  factor of  $\sim 100$  and overlapping the PL of the gain.

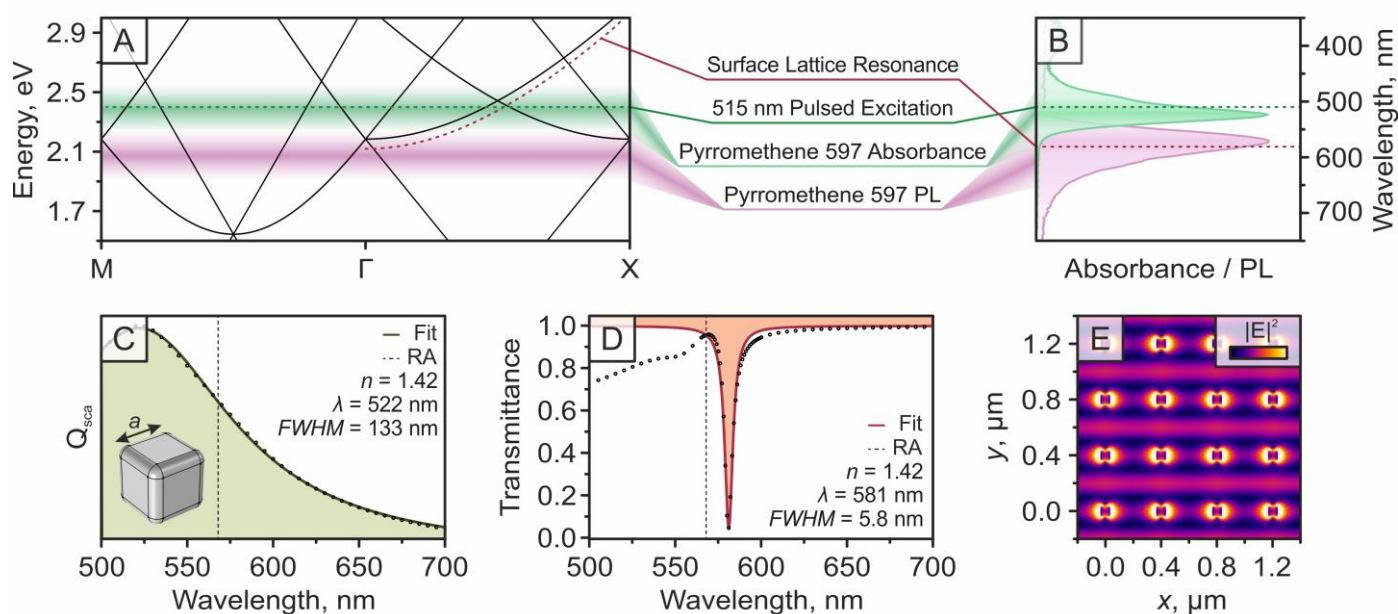


**Figure 2. Nanolaser design.** **A)** Empty square lattice band structure ( $\Lambda = 400$  nm,  $n = 1.42$ ) with an indicated SLR location (dashed red line) forming a flat band at the  $\Gamma$  point. Nanolaser pumping wavelength is indicated by a dashed green line, overlapping the absorbance of the dye. **B)** The photoluminescence and absorbance of the gain (P597 laser dye). **C)** Calculated scattering cross-section spectrum of  $a = 65$  nm edge length Ag nanocubes. Vertical dashed line indicates the location of the RA at the  $\Gamma$  point. **D)** Calculated transmittance spectrum of Ag nanocubes in the array (shaded curve is a Lorentzian fit and the location of the Rayleigh anomaly is indicated by a vertical dashed line). **E)** Calculated electric field intensity distribution of Ag nanocubes in the array at the SLR wavelength ( $\lambda = 581$  nm) when illuminated by a normally incident, x-polarized plane wave.

**Nanolaser fabrication.** We used CAPA to position the synthesized (see supplementary material for synthesis method) colloidal nanoparticles with single-particle resolution.<sup>40</sup> To use this technology, a patterned template is required, which we produce by molding a PDMS replica from a silicon master prepared by common nanofabrication routines (**Figure 3A**). A distinct advantage is that the replication process can be repeated multiple times without compromising the structure, minimizing the need for expensive

lithography processes associated with nanofabrication while ensuring reproducibility (**Figure 3B**). A scheme of the CAPA deposition process is shown in **Figure 3C**, where the colloidal solution is injected between the PDMS template and a stationary glass slide. The template is then translated relative to the latter, and its temperature is elevated until nanoparticles accumulate at the meniscus. Under optimal conditions, the nanoparticles are trapped in the pattern on PDMS

with a single-particle resolution as the solution withdraws.

An SEM micrograph of an assembly is shown in **Figure 3D**. There is some unintended disorder within these arrays, similar to the purposely introduced disorder reported in previous work.<sup>25</sup> The measured extinction of the assembly (**Figure 3E**, red curve) still showed a high-quality SLR resonance ( $\lambda = 572$  nm,  $Q = 66$ ), which matches the calculation in **Figure 2D** and overlaps the gain PL (**Figure 3E**, pink curve).

After assembly, the substrates are preemptively soaked in a 5 mM P597 solution in DMSO:EtOH (2:1) overnight, improving stability and preventing dye diffusion into PDMS during experiments (**Figure 3C**). Finally, a drop of dye

solution is placed on the substrate and covered with a cover slip. We found that the nanoparticles stay in place because the trap size is very close to the dimensions of the particles, leaving no room for movement and even requiring substantial persuasion to remove them.

**Figure 3F** shows the experimental setup to evaluate nanolasing characteristics. We pump our devices with a collimated, Yb:KGW second harmonic 515 nm wavelength, 2.4 mm ( $1/e^2$ ) size beam spot with a controlled linear polarization state. We used 50 Hz frequency to avoid excessive dye bleaching and collect normal emission from the sample in free space using a fiber-coupled spectrograph and a CMOS camera.

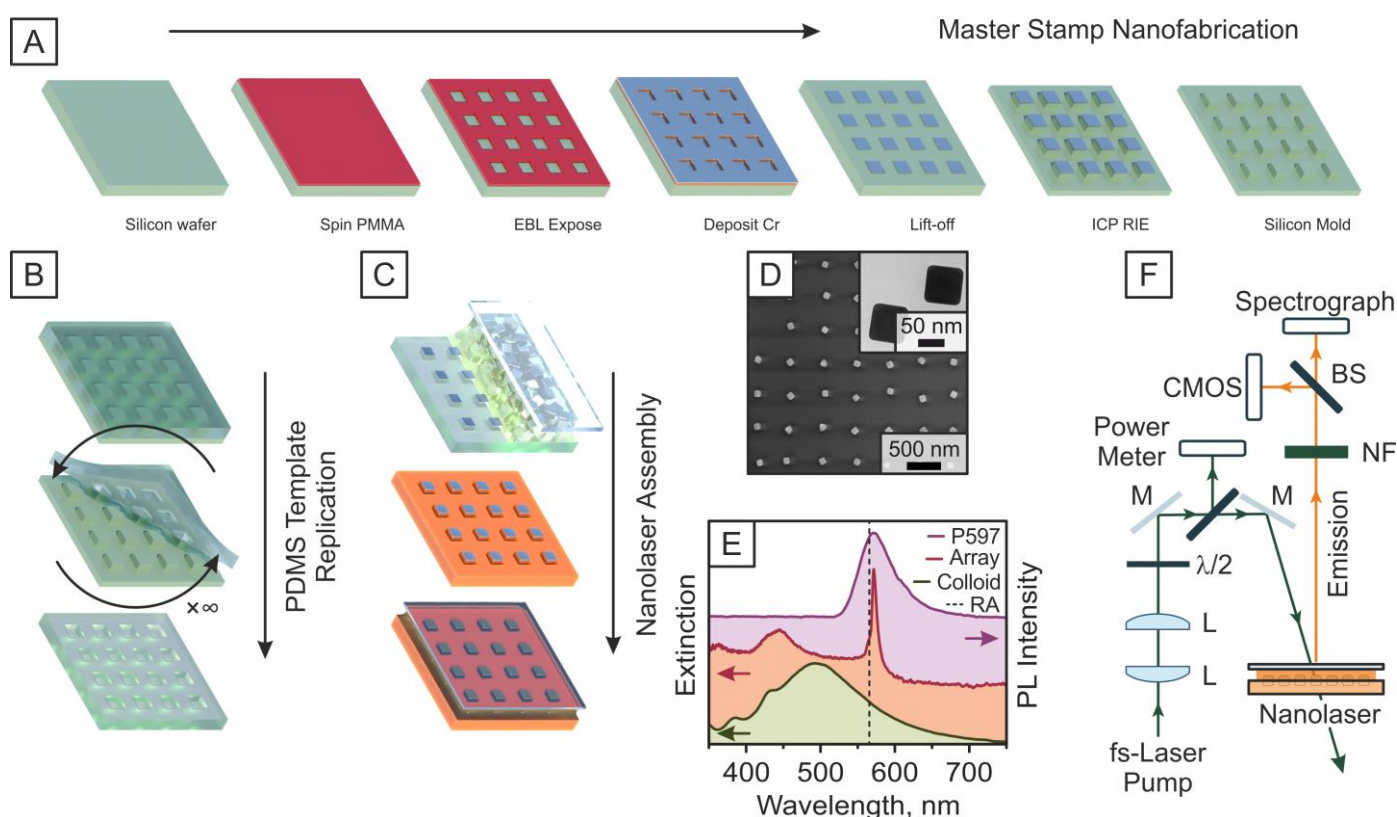


**Figure 3. Nanolaser fabrication based on nanoparticle self-assembly.** **A)** A master stamp is designed for a lattice resonance at a target wavelength and fabricated following standard lithography patterning and etching routines. **B)** The pattern is transferred to a PDMS film via soft-lithography and this process can be repeated many times, providing templates for numerous devices. **C)** Ag nanocubes featuring a LSPR close to the target wavelength are assembled into the template using CAPA. The devices are then soaked in a dye solution before being interfaced with an additional drop on top, confined by a glass cover slip. **D)** An SEM micrograph of assembled nanocubes in a PDMS template. Inset shows a TEM micrograph of the nanocubes. **E)** Experimental spectra of nanocubes in solution vs. in array, and the PL spectrum of the dye. The vertical dashed line indicates the location of the RA at the  $\Gamma$  point in PDMS. **F)** The nanolasers are characterized after pumping with a 270 fs 515 nm laser using a spectrograph and a CMOS camera (L – beam reducer;  $\lambda/2$  – half-waveplate, M – mirrors, NF – neutral density and notch filters).

### Nanolaser characterization

Claims of lasing typically require three key features indicating the required level of spectral and temporal coherence of the emitted light: (i) a clear threshold of pumping power beyond which the slope

of the input-output curve changes; (ii) a significant narrowing of the PL peak as the system crosses the lasing threshold, indicating the transition from spontaneous to stimulated emission; (iii) the emitted light must form a beam typical of the resonator.<sup>41</sup>

**Figure 4** summarizes our results regarding each of these points.

*Threshold and linewidth.* We ran all characterization experiments using two pump polarizations: TM and TE, schematically shown in **Figure 4A** and **E**, respectively. The characterization of lasing threshold is shown in **Figure 4B, F**. As the pump fluence increased above the threshold value, the intensity of the emission increased faster than that of the PL emission background, which is attributed to the nonlinearity associated with stimulated emission. The PL intensity before threshold is very small in our data because of how the experiment is set up – the spectrograph is coupled with a low-NA fiber coupler and located far from the sample, effectively eliminating all highly divergent PL signal. We recorded a threshold of  $80 \mu\text{J}/\text{cm}^2$  using both polarizations by repeatedly scanning the fluence close to the threshold to acquire more data points. We believe we achieve this competitive threshold compared to reports of similar systems<sup>11,21,29,32,42,43</sup> despite the unideal nanoparticle lattice because of enhanced plasmonic nanoparticle qualities enabled by monocrystallinity and low facet roughness, which decrease if not eliminate electron scattering at crystal boundaries and associated absorptive damping.<sup>28</sup>

The rapid increase in intensity beyond the threshold is accompanied by the emergence of a narrow peak around the SLR wavelength, suggesting the onset of lasing (**Figure 4C, G**). Lasing occurred close to the flat band edge ( $\sim 574 \text{ nm}$ ) of the lattice as intended (**Figure 2A**). We observed slight wavelength variations because of the open cavity system, leading to instability of the refractive index environment during the experiment, *i.e.*, evaporation and diffusion of the dye solvent. The PL linewidth

starts at  $\sim 45 \text{ nm}$  FWHM (**Figure 2B**) and rapidly decreases above the threshold to  $< 1.2 \text{ nm}$ , limited by our spectrograph resolution. In some cases, we observe a slight increase of linewidth with pumping power, but this is not uncommon for similar nanolasers.<sup>42</sup> Spectral narrowing is a telltale sign of temporal coherence, although a better evaluation is using the second-order correlation function  $g^{(2)}$ . Unfortunately, this measurement was not available at this time, and even if it was, it is challenging to acquire accurate results for a plasmonic nanolaser with gain materials composed of organic dye.<sup>7</sup>

*Beam profile and polarization.* The images of the laser beam were taken above the threshold by placing a CMOS camera at varying distances. **Figure 4D, H** shows these images taken at 22.5 cm for the two orthogonal polarizations, converted to angular coordinates (images at different distances are shown in **Figure S1**). In both cases, the beam consists of a multitude of horizontal or vertical lines, indicating that the device operates similarly to 1D distributed feedback (DFB) lasers.<sup>30,44</sup> We believe that the number and density of lines are associated with the quality of the nanoparticle lattice. We measured  $1/e^2$  of the narrow dimension of one of the lines (which remains almost constant at varying distances) profile in angular coordinates and estimated the divergence of individual lines to  $< 1 \text{ mrad}$ .

The output beam of the nanolaser above the threshold was strongly linearly polarized and followed one of the square lattice directions. If the polarization of the exciting beam did not match the lattice orientation, the emission still did, with variations in intensity corresponding to the projection of the electric field vector of the pump onto the lattice direction. A characterization of the polarization state is displayed in **Figure S2**.

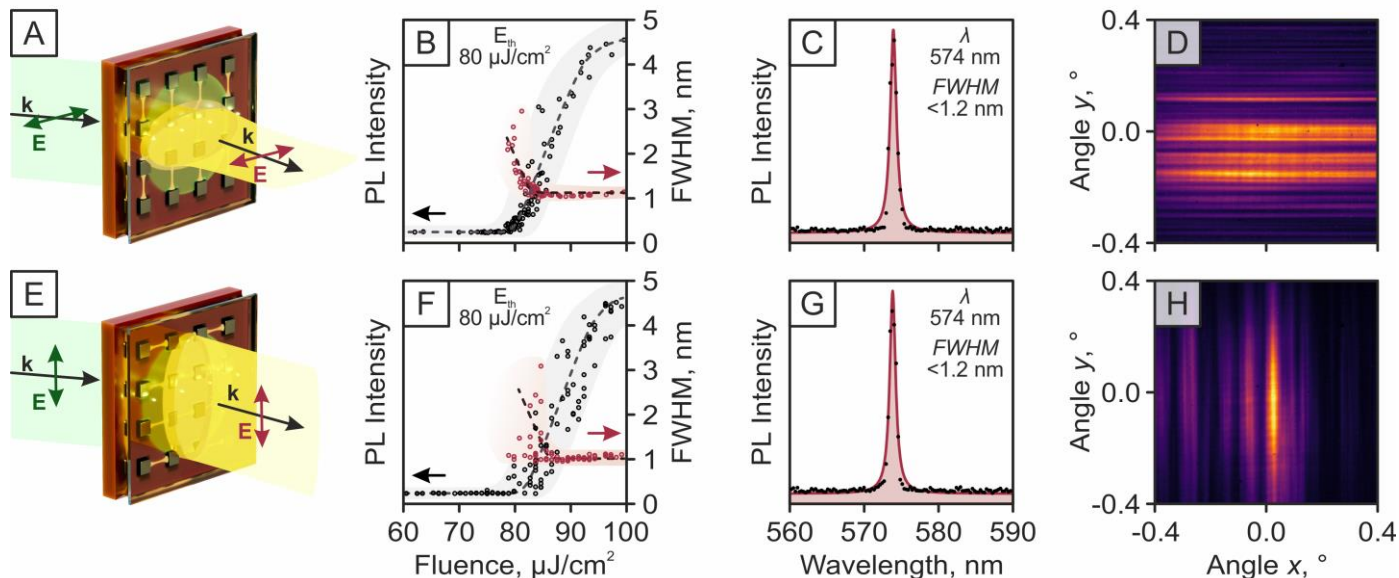


**Figure 4. Nanolaser characteristics.** **A, E)** The nanolaser emits a beam that follows the polarization of the pump and is extended in the same direction. **B, F)** the dependence of emission intensity and the FWHM of the lasing peak on the pumping fluence, exhibiting a clear threshold behavior. **C, G)** Emission spectra collected normal to the nanolaser plane above the lasing threshold. **D, H)** The beam profile of the nanolaser in angular coordinates captured by a CMOS camera 22.5 cm away from the device with no collection optics.

## Discussion

Apart from the characteristics discussed above, other phenomena similar to lasing must be ruled out.<sup>41,45,46</sup> Specifically, amplified spontaneous emission (ASE) can appear similar to lasing. It involves the stimulated amplification of PL by a single pass through the gain volume, irrespective of the feedback mechanism.<sup>47</sup> This effect can especially be difficult to discriminate against lasing if the designed wavelength is very close to the PL peak of the emission, such as in our case (**Figure 2B**). Like lasing, ASE can show a threshold behavior (albeit weaker and less consistent), linewidth narrowing, and produce somewhat directional emission. But the FWHM is usually in the range of a couple of tens of nm, the emitted wavelength does not depend on resonator configuration and the emission is unpolarized, contrary to the data presented here.

In our results, the FWHM is consistently  $< 1.2$  nm, which is the resolution limit of our spectrograph. We also tested our setup using a slightly different resonator (420 nm lattice, same nanocubes). The lasing peak followed this change (**Figure S3**), indicating that emission strongly depends on the resonator. Moreover, the beam our devices emit is clearly linearly polarized and follows the resonator geometry. Finally, in some cases we could observe the emergence of ASE at higher pumping powers, when it starts to outcompete lasing (**Figure S4**). This observation allows us to

unambiguously distinguish between these emission modes.

Another process that may be mistaken for lasing is the edge-emission of waveguided modes. In this case, the threshold behavior is unexpected, which we consistently observe in our system. Moreover, we collect our data at the normal to the device surface. 1D distributed feedback (DFB) lasers emit elongated beams with low divergence along the feedback axis and high divergence perpendicular to it, which emerges as a fan-like beam.<sup>41,48</sup> We observe similar fan-like emission with orientation aligned to one of the lattice directions. This observation strongly suggests that the 2D array of nanoparticles essentially behaves as a collection of 1D arrays and emits a set of these fan-like beams. Plasmonic nanoparticles predominantly support electric modes, and dipolar electric modes mainly radiate, couple, and provide feedback in directions orthogonal to the axis of the induced dipole. 2D feedback and annular beams can be achieved by simultaneously providing TM and TE excitation by switching to waveguide-hybridized SLR modes (nanoparticles on a thin film)<sup>16</sup> or high-NA objective-based excitation.<sup>49</sup>

Finally, we left our devices operating and measured the expected lifetime (**Figure S5**). Although we were using an open system and a liquid dye solution, these nanolasers still maintained narrow linewidth emission for 15-30 minutes,

depending on polarization. TE configuration extended the lifetime approx. 2-fold, but at a lower overall intensity. Replacement of the dye solution allows the used devices to regenerate and they can be operated again, indicating that the resonator is not damaged and the nanoparticles stay in place.

Overall, the demonstrated results clearly show that the emission from our devices strongly corresponds to the resonator used with a clearly defined threshold and polarization state. Therefore, our experimental observations strongly favor the claim of nanolasing from these assembled colloidal nanocube arrays.

## Conclusions

We presented a novel approach to develop a surface lattice resonance-based plasmonic nanolaser with competitive characteristics. We used a template-assisted technique to assemble highly crystalline silver colloidal nanocubes into periodic arrays. These plasmonic substrates featured a high-quality SLR, which served as a feedback mechanism for stimulated emission. We demonstrated a nanolaser with a narrow linewidth of  $<1.2$  nm, a lasing threshold of  $<100$   $\mu\text{J}/\text{cm}^2$ , and a beam characteristic of the resonator with minimal divergence and a clear polarization state. We claim that our devices are comparable to lithography-made counterparts by exploiting the enhanced emission by defects in the lattice while maintaining a low threshold and scalability. These attributes, coupled with the potential for large-scale production leveraging colloidal methods and template-assisted assembly techniques, position our devices as promising candidates for applications. Such plasmonic arrays can be inexpensively transferred onto almost any substrate, allowing easy integration in applications ranging from point-of-care diagnostics to photonic integrated circuits and optical communications systems.

## Acknowledgements

This research was performed within project "LaSensA" under the M-ERA.NET scheme and was funded by the Research Council of Lithuania (LMTLT), agreement No. S-M-ERA.NET-21-2, National Science Centre (Poland), agreement No. UMO-2020/02/Y/ST5/00086, Saxon State Ministry for Science, Culture and Tourism (Germany) and co-financed with tax funds on the basis of the budget passed by the Saxon state parliament. JH thanks the Japan

Society for the Promotion of Science (JSPS) Grants-in-Aid for Scientific Research Kakenhi Program (20K05453).

## Author details

<sup>1</sup> Institute of Materials Science, Kaunas University of Technology, K. Baršausko St. 59, LT-51432 Kaunas

<sup>2</sup> Research Center for Materials Nanoarchitectonics (MANA), National Institute for Materials Science (NIMS), 1-1 Namiki, Tsukuba, Ibaraki 305-0044, Japan

\* Corresponding author:

Mindaugas Juodėnas, mindaugas.juodenas@ktu.lt

## Author contributions

MJ: research idea and supervision, calculations, experimental design, experimental work, data analysis, draft writing; NK: experimental design, experimental work, data analysis, draft writing; GK: experimental work, draft writing; JH: research idea and experimental work; TT: experimental design; ST: research supervision. All authors contributed to the editing of the final draft.

## Data availability

Data supporting the findings of this study are available from the corresponding author on a reasonable request.

## Competing interests

The authors declare no competing interests.

## Supplementary information

The document contains supplementary material.

## References

1. Liang, Y., Li, C., Huang, Y.-Z. & Zhang, Q. Plasmonic Nanolasers in On-Chip Light Sources: Prospects and Challenges. *ACS Nano* **14**, 14375–14390 (2020).
2. Ma, R.-M. & Oulton, R. F. Applications of nanolasers. *Nat. Nanotechnol.* **14**, 12–22 (2019).
3. Meinzer, N., Barnes, W. L. & Hooper, I. R. Plasmonic meta-atoms and metasurfaces. *Nat. Photonics* **8**, 889–898 (2014).
4. Utyushev, A. D., Zakomirnyi, V. I. & Rasskazov, I. L. Collective lattice resonances: Plasmonics and beyond. *Rev. Phys.* **6**, 100051 (2021).
5. Guan, J. *et al.* Light–Matter Interactions in Hybrid Material Metasurfaces. *Chem. Rev.* **122**, 15177–15203 (2022).
6. Vaskin, A., Kolkowski, R., Koenderink, A. F. & Staude, I. Light-emitting metasurfaces. *Nanophotonics* **8**, 1151–1198 (2019).
7. Zhou, W. *et al.* Lasing action in strongly coupled plasmonic nanocavity arrays. *Nat. Nanotechnol.* **8**, 506–511 (2013).

8. Schokker, A. H. & Koenderink, A. F. Lasing at the band edges of plasmonic lattices. *Phys. Rev. B* **90**, 155452 (2014).
9. Yang, A. *et al.* Real-time tunable lasing from plasmonic nanocavity arrays. *Nat. Commun.* **6**, 6939 (2015).
10. Wang, D. *et al.* Stretchable Nanolasing from Hybrid Quadrupole Plasmons. *Nano Lett.* **18**, 4549–4555 (2018).
11. Heilmann, R., Arjas, K., Hakala, T. K., & Päivi Törmä. Multimode Lasing in Supercell Plasmonic Nanoparticle Arrays. *ACS Photonics* **10**, 3955–3962 (2023).
12. Freire-Fernández, F. *et al.* Quasi-Random Multimetallic Nanoparticle Arrays. *ACS Nano* **17**, 21905–21911 (2023).
13. Hakala, T. K. *et al.* Lasing in dark and bright modes of a finite-sized plasmonic lattice. *Nat. Commun.* **8**, 13687 (2017).
14. Freire-Fernández, F. *et al.* Magnetic on–off switching of a plasmonic laser. *Nat. Photonics* **16**, 27–32 (2022).
15. Guan, J. *et al.* Engineering Directionality in Quantum Dot Shell Lasing Using Plasmonic Lattices. *Nano Lett.* **20**, 1468–1474 (2020).
16. Guan, J. *et al.* Quantum Dot-Plasmon Lasing with Controlled Polarization Patterns. *ACS Nano* **14**, 3426–3433 (2020).
17. Yadav, R. K. *et al.* Room Temperature Weak-to-Strong Coupling and the Emergence of Collective Emission from Quantum Dots Coupled to Plasmonic Arrays. *ACS Nano* **14**, 7347–7357 (2020).
18. Xing, D. *et al.* Ligand Engineering and Recrystallization of Perovskite Quantum-Dot Thin Film for Low-Threshold Plasmonic Lattice Laser. *Small* **18**, 2204070 (2022).
19. Fernandez-Bravo, A. *et al.* Ultralow-threshold, continuous-wave upconverting lasing from subwavelength plasmons. *Nat. Mater.* **18**, 1172–1176 (2019).
20. Guan, J. *et al.* Plasmonic Nanoparticle Lattice Devices for White-Light Lasing. *Adv. Mater.* **35**, 2103262 (2023).
21. Guan, J. *et al.* Far-field coupling between moiré photonic lattices. *Nat. Nanotechnol.* 1–7 (2023) doi:10.1038/s41565-023-01320-7.
22. Wang, W. *et al.* Ultrafast Dynamics of Lattice Plasmon Lasers. *J. Phys. Chem. Lett.* **10**, 3301–3306 (2019).
23. Henzie, J., Lee, M. H. & Odom, T. W. Multiscale patterning of plasmonic metamaterials. *Nat. Nanotechnol.* **2**, 549–554 (2007).
24. Schokker, A. H. & Koenderink, A. F. Lasing in quasi-periodic and aperiodic plasmon lattices. *Optica* **3**, 686–693 (2016).
25. Schokker, A. H. & Koenderink, A. F. Statistics of Randomized Plasmonic Lattice Lasers. *ACS Photonics* **2**, 1289–1297 (2015).
26. Juodėnas, M., Tamulevičius, T., Henzie, J., Erts, D. & Tamulevičius, S. Surface Lattice Resonances in Self-Assembled Arrays of Monodisperse Ag Cuboctahedra. *ACS Nano* **13**, 9038–9047 (2019).
27. Tao, A. R., Habas, S. & Yang, P. Shape Control of Colloidal Metal Nanocrystals. *Small* **4**, 310–325 (2008).
28. Khinevich, N. *et al.* Size and crystallinity effect on the ultrafast optical response of chemically synthesized silver nanoparticles. *J. Materiomics* **10**, 594–600 (2024).
29. Deng, S. *et al.* Ultranarrow plasmon resonances from annealed nanoparticle lattices. *Proc. Natl. Acad. Sci.* **117**, 23380–23384 (2020).
30. Knudson, M. P. *et al.* Polarization-Dependent Lasing Behavior from Low-Symmetry Nanocavity Arrays. *ACS Nano* **13**, 7435–7441 (2019).
31. Karanikolas, V. *et al.* Plasmon-Triggered Ultrafast Operation of Color Centers in Hexagonal Boron Nitride Layers. *ACS Omega* **8**, 14641–14647 (2023).
32. Conti, Y., Passarelli, N., Mendoza-Carreño, J., Scarabelli, L. & Mihi, A. Colloidal Silver Nanoparticle Plasmonic Arrays for Versatile Lasing Architectures via Template-Assisted Self-Assembly. *Adv. Opt. Mater.* **11**, 2300983 (2023).
33. Henzie, J., Andrews, S. C., Ling, X. Y., Li, Z. & Yang, P. Oriented assembly of polyhedral plasmonic nanoparticle clusters. *Proc. Natl. Acad. Sci.* **110**, 6640–6645 (2013).
34. Juodėnas, M. *et al.* Effect of Ag Nanocube Optomechanical Modes on Plasmonic Surface Lattice Resonances. *ACS Photonics* **7**, 3130–3140 (2020).



35. AL-Aqmar, D. M., Abdelkader, H. I. & Abou Kana, M. T. H. Optical, photo-physical properties and photostability of pyrromethene (PM-597) in ionic liquids as benign green-solvents. *J. Lumin.* **161**, 221–228 (2015).
36. Partridge, W. P., Laurendeau, N. M., Johnson, C. C. & Steppel, R. N. Performance of Pyrromethene 580 and 597 in a commercial Nd:YAG-pumped dye-laser system. *Opt. Lett.* **19**, 1630–1632 (1994).
37. Hu, Z. *et al.* Coherent Random Fiber Laser Based on Nanoparticles Scattering in the Extremely Weakly Scattering Regime. *Phys. Rev. Lett.* **109**, 253901 (2012).
38. Yariv, E., Schultheiss, S., Saraidarov, T. & Reisfeld, R. Efficiency and photostability of dye-doped solid-state lasers in different hosts. *Opt. Mater.* **16**, 29–38 (2001).
39. Peckus, D. *et al.* Hot Electron Emission Can Lead to Damping of Optomechanical Modes in Core-Shell Ag@TiO<sub>2</sub> Nanocubes. *J. Phys. Chem. C* **121**, 24159–24167 (2017).
40. Kraus, T. *et al.* Nanoparticle printing with single-particle resolution. *Nat. Nanotechnol.* **2**, 570–576 (2007).
41. Samuel, I. D. W., Namdas, E. B. & Turnbull, G. A. How to recognize lasing. *Nat. Photonics* **3**, 546–549 (2009).
42. Rekola, H. T., Hakala, T. K. & Törmä, P. One-Dimensional Plasmonic Nanoparticle Chain Lasers. *ACS Photonics* **5**, 1822–1826 (2018).
43. Hoang, T. B., Akselrod, G. M., Yang, A., Odom, T. W. & Mikkelsen, M. H. Millimeter-Scale Spatial Coherence from a Plasmon Laser. *Nano Lett.* **17**, 6690–6695 (2017).
44. Yoshida, K. *et al.* Electrically driven organic laser using integrated OLED pumping. *Nature* **621**, 746–752 (2023).
45. Scrutinizing lasers. *Nat. Photonics* **11**, 139–139 (2017).
46. Sato, R. *et al.* Random Lasing via Plasmon-Induced Cavitation of Microbubbles. *Nano Lett.* **21**, 6064–6070 (2021).
47. Kuehne, A. J. C. & Gather, M. C. Organic Lasers: Recent Developments on Materials, Device Geometries, and Fabrication Techniques. *Chem. Rev.* **116**, 12823–12864 (2016).
48. Samuel, I. D. W. & Turnbull, G. A. Organic Semiconductor Lasers. *Chem. Rev.* **107**, 1272–1295 (2007).
49. Heliotis, G. *et al.* Emission Characteristics and Performance Comparison of Polyfluorene Lasers with One- and Two-Dimensional Distributed Feedback. *Adv. Funct. Mater.* **14**, 91–97 (2004).

# Lasing in an Assembled Array of Silver Nanocubes

Mindaugas Juodėnas<sup>1</sup>, Nadzeya Khinevich<sup>1</sup>, Gvidas Klyvis<sup>1</sup>,  
Joel Henzie<sup>2</sup>, Tomas Tamulevičius<sup>1</sup>, Sigitas Tamulevičius<sup>1</sup>

## Supplementary information

### Materials and methods

#### Nanoparticle synthesis

Monodisperse solutions of Ag nanocubes were prepared using a modified procedure based on the polyol synthesis method described in *J. Phys. Chem. C*; **121**, 24159-24167 (2017). 80 mg of copper chloride (CuCl<sub>2</sub>) was dissolved in 10 g of 1,5-pentanediol (PD; Acros). Next, 0.4 g of polyvinylpyrrolidone (PVP; Sigma-Aldrich) was dissolved in 20 g of PD by sonication. And in a separate vial, 35 μL of the above CuCl<sub>2</sub> solution and 0.4 g of AgNO<sub>3</sub> was dissolved in 20 g of PD via sonication. Next, 20 g of PD was added to a 100 mL round bottom flask (RBF) and heated to an internal temperature of 130 °C. Once the PD reached 130 °C, 500 μL of the AgNO<sub>3</sub> solution was added to the RBF, then 30 s later 500 μL of the PVP solution was added to the RBF. This procedure was repeated every minute (i.e. add the Ag<sup>+</sup> solution at 0:00, the PVP solution at 0:30, then Ag<sup>+</sup> at 1:00, and so forth) until the nanocubes achieved the desired size. The Ag nanocubes used in this study had an average edge length (*a*) of 77 ± 3 nm, measured across 200 nanoparticles using a JEOL-1010 Transmission Electron Microscope (TEM) set at 100 kV with a resolution of 0.5 nm/pixel. These particles were dispersed in DMF at a concentration of 3.59 × 10<sup>11</sup> particles per milliliter, as confirmed by inductively coupled plasma atomic emission spectrometry. During the synthesis, each Ag nanocube is coated with a polyvinylpyrrolidone (PVP; molecular weight 55,000) surfactant layer, which acts as a steric barrier to prevent excessive aggregation when particle concentrations are high.

#### Simulations

Finite element method (FEM) modeling was performed using COMSOL Multiphysics using the wave optics module. Samples were modeled by building a unit cell with Floquet boundary conditions. The array was illuminated from a port below the nanoparticles; a second port above collected the transmitted light. The dielectric function was used from Johnson & Christy data (*Phys. Rev. B*; **6**, 4370 (1972)).

#### Fabrication of the SLR-based resonator

Capillary-assisted particle assembly deposition on PDMS replica was performed using a custom setup equipped with a motorized linear precision translator (LS-110, PI Micos), a temperature control system (TEC-1090, Meerstetter Engineering GmbH), and an optical microscope system (BX51, Olympus) with a CCD camera (Micropublisher 3.3, QImaging). The PDMS templates are produced by molding the structure from a silicon master nanofabricated using e-beam lithography (eLine Plus, Raith) and inductively coupled plasma reactive ion etching (Apex SLR, Plasma-Therm). The templates were placed on the moving stage, and 100 μL of silver nanocube solution was injected and confined by a fixed microscope slide. The drop of solution moved along the surface with a stage speed of 3.3 μm/s, forming the meniscus. Evaporation-induced flux and the contact angle led to nanocubes accumulating at the edge of the meniscus and filling the traps. The temperature of the sample holder is controlled by the thermoelectric controller and was set at 13.2°C above the dew point.

#### Nanolaser architecture

To realize lasing emission from these NP cavities, we used pyromethene 597 dye (Exciton) as gain material. The dye was dissolved in DMSO:Ethanol in a ratio of 2:1 to achieve index matching at *n*=1.42. The concentration of the dye was 5 mM. The nanoparticle arrays were submerged into this solution to allow the dye to penetrate PDMS

and surround the nanoparticles. Before experiments, a drop of dye solution (10  $\mu\text{l}$ ) was placed on the substrate and covered by a glass cover slip.

### Nanolasing measurements

The nanolaser was pumped by the 2<sup>nd</sup> harmonic (515 nm) of 290 fs pulse length Yb:KGW laser Pharos (Light Conversion) at a 40 kHz repetition rate at room temperature. The pulse picker was set to transmit every 800<sup>th</sup> pulse to effectively reduce the frequency to 50 Hz. The pump beam was reduced to a 1.4 mm FWHM diameter spot (2.38 mm  $1/e^2$ ) on the sample at an incident angle of *ca.* 22°. The emission spectra were collected at the normal to the sample surface using a home-built experimental setup. Optical characterization of the fabricated template demonstrated SLR and lasing emission were registered using a fiber-optic spectrograph AvaSpec-2048 (Avantes) with a 1.2 nm resolution in the 400–800 nm spectral range. The spatial pattern and divergence angle of the lasing beam were analyzed using a beam profiler WinCamD-LCM (DataRay Inc.) equipped with a 1" CMOS sensor and placed normal to the sample surface on an optical rail.

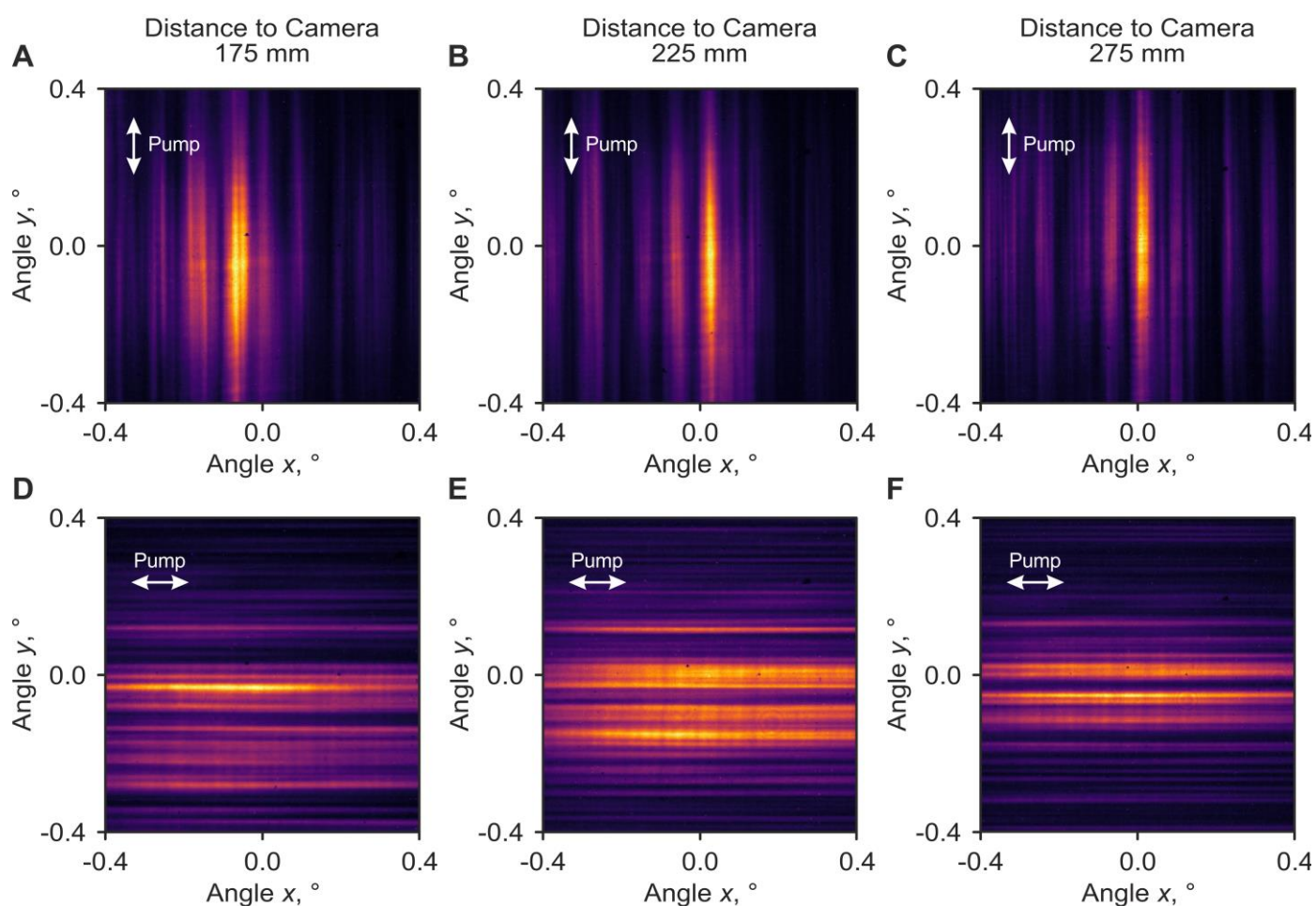


**Figure S1.** Camera images of the emitted beam were taken at varying distances from the nanolaser (indicated above), and two characteristic polarizations are indicated in the top left of each image.

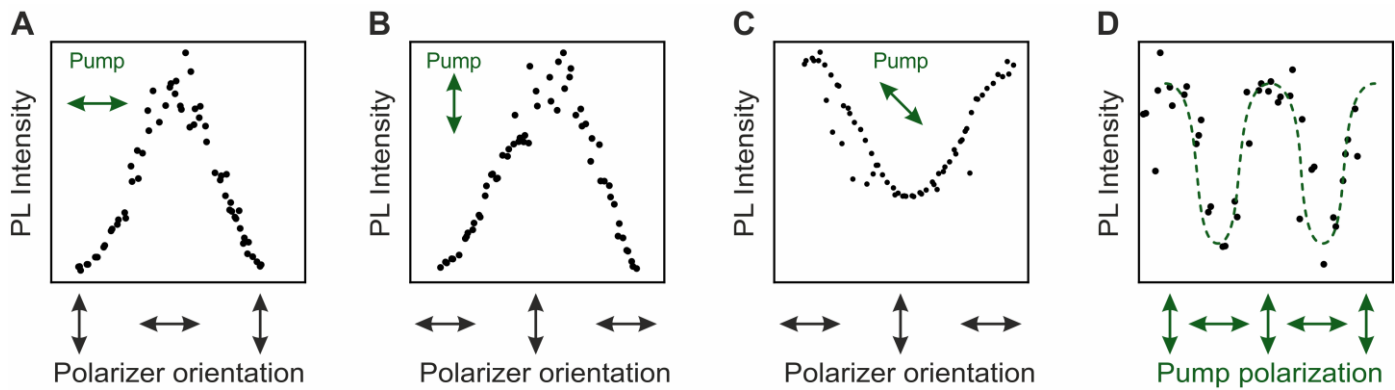


**Figure S2.** The polarization of the emitted beam was characterized by placing a linear polarizer between the nanolaser and the spectrometer. Measurements were done by rotating the polarizer when pumping with TM (a), TE (b), and 45° (c) polarized light. Finally, the polarizer after the nanolaser was removed and the polarization of the pump was rotated continuously (d).

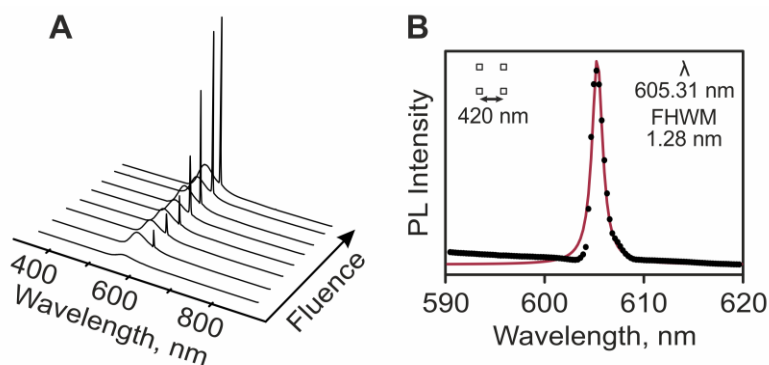


**Figure S3.** Nanolaser emission with a 420 nm periodicity SLR system. The device shows threshold behavior and linewidth narrowing (a), and emission is centered at 605 nm (b), consistent with the change of the flat band shift (RA is calculated at 420 nm x 1.42 = 596.4 nm)

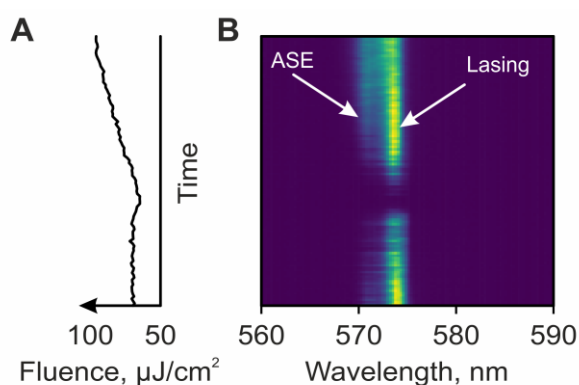


**Figure S4.** In some cases, higher intensity pumping (a) results in the rise of amplified spontaneous emission as a broader shoulder next to the lasing peak (b).

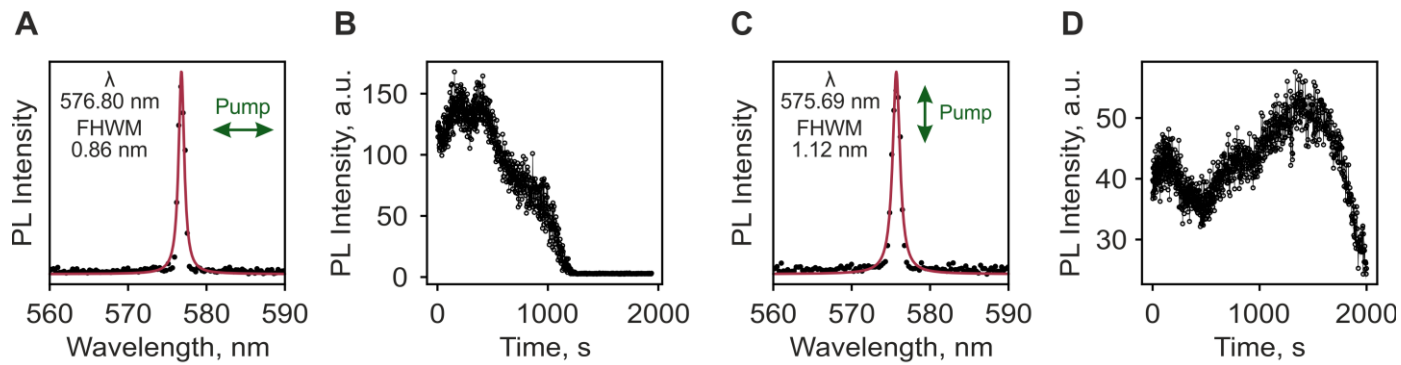


**Figure S5.** Long-term measurement of the nanolaser using orthogonal polarizations. a, b) TM polarization, the device lased for  $\sim 1000$  s; c, d) TE polarization, the device lased for  $>2000$  s, albeit at a lower intensity.